Astronomical and Astrophysical Transactions (*AApTr*), 2024, Vol. 34, Issue 4, pp. 343–362,
ISSN 1055-6796, Photocopying permitted by license only, ©Cambridge Scientific Publishers

Dynamic processes in jets of AGNs on the VLBA (MOJAVE) data

D. Zabora*, M. Ryabov, A. Sukharev

Odesa Observatory URAN-4, Institute of Radio Astronomy of the National Academy of Sciences of Ukraine (IRA NASU), Marzalievska Str., 1B, Odesa, 65000, Ukraine

Received 24 October, 2024; accepted 31 October, 2024

MOJAVE is one of the most effective VLBI monitoring programs to observe Active Galactic Nuclei (AGN) jets angular structure in the radio band. MOJAVE uses the radio interferometric network of 10 radio telescopes of the National Radio Astronomy Observatory (NRAO, USA).

Observation results are available in the MOJAVE Database (MOJAVE/2cm Survey Data Archive). With the largest database of about 8600 km, the system allows mapping AGN's close surroundings at ∼0.12 mas resolution on ∼15.4 GHz frequency.

For approximately 30 years of MOJAVE AGN monitoring observations, the Survey Data Archive accumulated a huge amount of observation data. Especially interesting are data about the locations of bright features (components) in jets and their changes in time. This data is presented in image format (separation vs. time plot). And their presence allows us to analyze motion patterns of components in jets, which represent AGN's activity, as well as the jet's structure itself.

This work analyzed the motion of components in the Seyfert I galaxy 3C 120 (1995.6–2020 yy, 54 components),

Quasars 3C 273 (1995.6–2020 yy, 31 components) and 3C 454.3 (1995.4–2019 yy, 9 components), BL Lac (1995.3–2020 yy, 37 components) was performed. These objects demonstrate presence both of moving and quasi-stationary components, which slowly change their locations in time. Based on the moving components, the average velocities and accelerations in the jets were estimated in projection onto the picture plane. Also, the distribution of velocities of the components in the jets was constructed and assumptions were made about the structure of the jets based on existing publications on them.

The discussed components demonstrate inhomogeneities in their movement up to quasi-harmonic oscillations of their positions relative to the average movement direction trend. Especially interesting are the oscillations of quasi-stationary components close to nuclei, which can be a result of the propagation of shock waves in jets.

Keywords: Galaxies: active, galaxies: jets, kinematics: jets, radio continuum: galaxies

*Email: zaboradaniil@gmail.com

1 Introduction

Active processes in AGN lead to a variable nature of radio emission and their spatial structure. The primary process in AGN emission and jet formation is the accretion of matter from the accretion disk onto the black hole, and a change in the accretion rate onto the black hole will affect the change in the radio flux [1] (and the frequency of ejection of bright components). The presence of a second companion black hole, perturbing the accretion disk, will cause jet precession [2], changing and complicating its spatial structure.

As a result of the core activity, relativistic plasma blobs are periodically ejected into the jet, shock waves and disturbances in the structure of the jet magnetic field arise, so electrons are additionally accelerated at the shock wave front. As a result, the jet emits synchrotron radiation [3], forming a radio image of the core and jet system (Fig. 1).

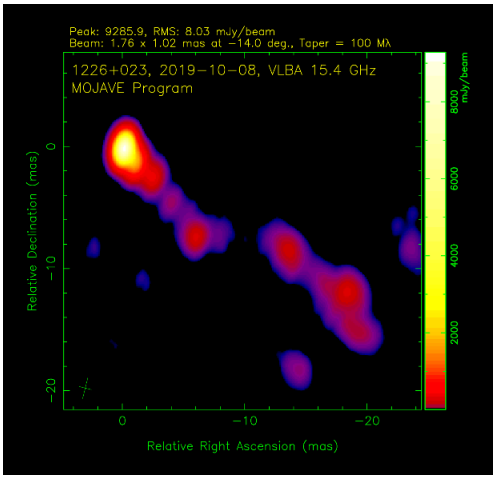


Figure 1 Radio image of 3C 273 obtained by the VLBA system.

Active galactic nuclei and their jets are not closed systems. The surrounding galaxy, intergalactic matter has a significant impact on the formation of the accretion disk and jet. The results of numerical calculations show that galactic matter feeds accretion onto a black hole, and extragalactic matter (as well as galactic matter) can slow down the jet matter, significantly shortening it, changing its direction relative to the initial one, or even stopping its formation [4].

2 MOJAVE monitoring program

The MOJAVE VLBI radio interferometric monitoring program uses the VLBA interferometer, a system of 10 25-meter radio telescopes of NRAO (Fig. 2). The VLBA system operates in 11 frequency bands (∼0.3, 0.6, 1.4, 1.7, 2.3, 5, 7.5, 15, 30, 43, 96 GHz). The resolution varies from 22 mas at 0.3 GHz to 0.12 mas at 96 GHz [5].

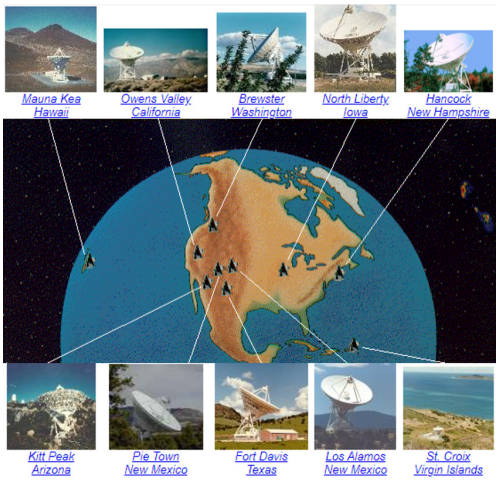


Figure 2 VLBA sites on the globe.

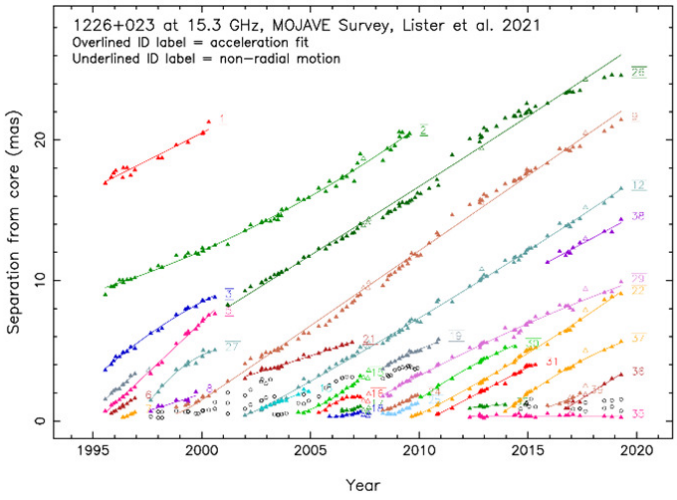


Figure 3 Separation vs time plot for 3C 273.

The MOJAVE project also has an open database [6] providing access to data on radio flux variations, radio images of nuclei and jets, and polarization maps for a sample of ∼514 active galactic nuclei at a frequency of ∼15 GHz. Time intervals between source observation sessions range from 5–10 days to a year. Important data provided by the MOJAVE team are the angular deviations of the bright components ejected into the jet from the core over time. They are presented in the form of a separation vs time plot (Fig. 3) available for most active galactic nuclei from the MOJAVE sample, based on which the motion of bright features (components in the jet) will be analyzed in this paper. Obtaining and processing of images is described in the MOJAVE papers [7–9].

3 The considered AGNs

In this work, the following active galactic nuclei were considered: 3C 120, 3C 273, 3C 454.3, BL Lac. Previously, we conducted studies of the variability of these objects according to the data of monitoring fluxes carried out at the Michigan Radio Astronomy Observatory at frequencies of 4, 8, and 15 GHz for a period of about 40 years [10–14]. We also used the MOJAVE data [15, 16].

3C 120 is a nearby bright AGN classified as a Seyfert Type I galaxy at redshift $z \sim 0.033$ [17]. A single black hole with a mass of $6 \times 10^7\ M_\odot$ is assumed to be in the core [18] (estimated by reverberation and spectroscopic methods). According to [19], the jet is formed predominantly from electron-positron pairs. The kinematics of the motion of bright components in the jet is considered in [20] based on MOJAVE data, which found that the velocity of the components increases from the core to ∼7 mas, after which it decreases. In [21], based on polarimetric data (Faraday effect), the possibility of the presence of a spiral structure of the magnetic field of 3C 120 is investigated. But despite the presence of a gradient in the Rotation Measure, the presence of a region of enhanced rotation and uncorrelated rotation measure in different regions of the jet hints that the plane of polarization rotates predominantly in the clouds on the line of sight, and not in the jet itself, so the spiral structure of the magnetic field in the jet remains questionable.

Quasar 3C 273 is one of the brightest and closest quasars, located in the constellation Virgo at $z \sim 0.1576$ [22]. The article [23] considers a model of a binary black hole with an estimate of the mass of its components: $M \sim 10^{10} M_\odot,\ m \sim 0.55 \cdot 10^{10} M_\odot$, which is in good agreement with spectroscopic and reverberation estimations [24].

In [25], the jet kinematics and its collimation failure are investigated, similar is presented in [26]. In [27], the jet was studied for the velocity gradient perpendicular to the axis and the non-ballistic motion of individual components, the stratification of the jet into an inner layer (with high speeds) and an outer layer (with lower speeds), a similar thing was observed in [20]. In [28], variations of the Lorentz factor in the jet 3C 273 are considered and models for description are proposed. In [21] the spiral structure of the magnetic field and the jet of 3C 273 is researched, in which the model with a spiral magnetic field is confirmed, and the matter in the jet accelerates with distance from the core.

Quasar 3C 454.3, sometimes classified as a blazar, is a loud radio source at $z \sim 0.859$ [29]. For it, binary black hole models are proposed based on quasi-periodic variations in the radio flux at different frequencies with an estimated component mass ratio of $m/M \sim 0.3$ and a total system mass of $\left[0.9 \cdot 10^{10} - 7.3 \cdot 10^{10}\right] M_\odot$, which is one of the most massive binary black holes known at present. A perturbation in the accretion disk caused by the presence of a second black hole is also considered [30]. In [31,32], a group of authors considers a model of a precessing jet based on the kinematics of the motion of bright components in it. The precession of the jet is explained by the presence of a binary black hole in the center with the same mass ratio. In addition, article [33] partially confirms the presence of a spiral magnetic field in the jet.

BL Lac is a blazar (BL Lacertae object, the first discovered object from the BL Lac objects) at redshift $z \sim 0.0686$ [34]. In [35], the lower limit of the black hole mass is found to be $\sim 3 \cdot 10^7 M_\odot$. In [36], based on MOJAVE data, the authors emphasize the

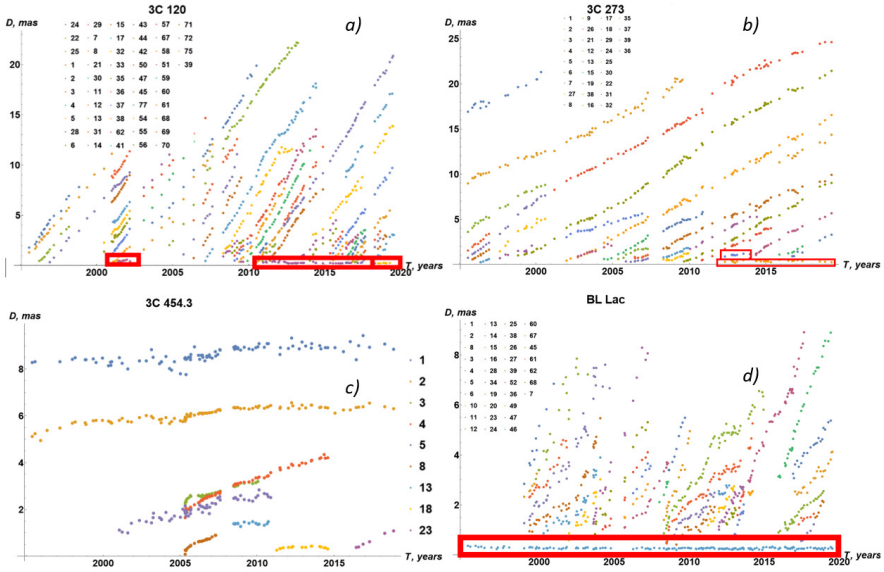


Figure 4 Reconstructed separation vs time plot: 3C 120 (a), 3C 273 (b), 3C 454.3 (c), BL Lac (d).

presence of a quasi-stationary component (7th according to the MOJAVE numbering), recording its quasi-periodic motion around the mean position (at a distance of $\sim$ 0.25 *mas* from the core) with an average amplitude of $\sim$0.03 mas and a characteristic time of $\sim$ 0.5 years.

In [37], the BL Lac jet is considered under the condition of helicity of the magnetic field in it, and the stationary component (7th) is assumed to be a recollimation shock in a magnetohydrodynamic jet. And the moving components, which can be seen in the radio images, are explained as the fronts of shock wave propagation (slow or fast MHD waves). Such an analysis is possible only in a jet with a dominant helical magnetic field, that is, one in which the magnetic pressure prevails over the pressure of the plasma flow. As for the helicity of the magnetic field, in [33, 38], taking into account the presence of Faraday rotation of the plane of polarization and consistency with the corresponding relativistic MHD simulations, the helicity of the magnetic field is confirmed, at least in the vicinity of the core. Additionally, in the article [38], due to the higher resolution (of the order of tens of microseconds), recollimation shocks are found even closer to the core.

The separation vs time diagrams, reconstructed from the original MOJAVE, for 3C 120 (54 components, 920 points), 3C 273 (31 components, 740 points), 3C 454.3 (9 components, about 410 points), BL Lac (37 components, 880 points) can be seen in Fig. 4.

The diagram for 3C 120 shows both moving and quasi-stationary components (21, 39, 75) according to the MOJAVE numbering (marked with a red rectangle, Fig. 4a). The diagram for 3C 273 shows both moving and quasi-stationary components (32, 35) according to the MOJAVE numbering (marked with a red rectangle, Fig. 4b). 3C 454.3 shows predominantly slow-moving components, with the smallest deviations

over time being demonstrated by components (13, 18), shown in Fig. 4c. The BL Lac jet consists predominantly of moving components with the exception of one quasi-stationary one (the 7th, marked with a red rectangle in Fig. 4d).

All of the listed AGNs were observed by the MOJAVE project from 1995 to the present day, however the separation vs time data are presented over a time period (1995–2020).

4 Investigation

For each component of the considered AGN, smoothing was performed by three points (to reduce the number of random and instrumental errors). Then, using the smoothed data, the average velocity of each component was obtained by linear interpolation and the average acceleration (for components with five or more observation epochs); an example can be found in Fig. 5.

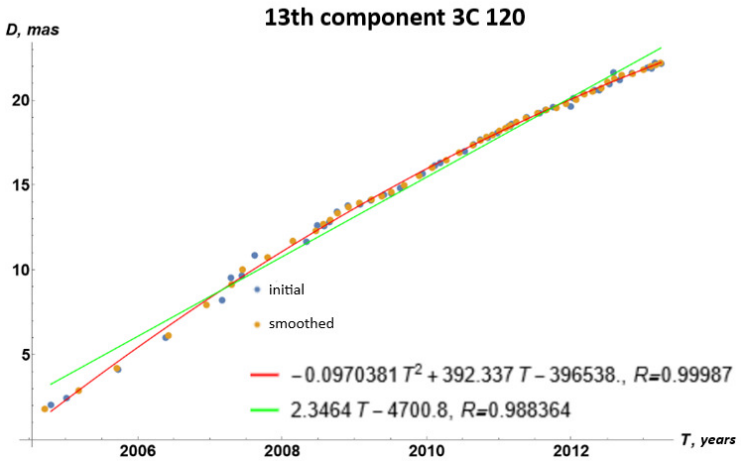


Figure 5 Angular deviation of the 13th component of 3C 120 over time: blue indicates the original data, orange indicates the smoothed data, green and red indicate the linear and quadratic approximations.

Thus, the average velocities and accelerations of jets (as the average value of the velocities and accelerations, respectively, of the moving components in the jets) of the sources 3C 120, 3C 273, 3C 454.3, BL Lac were calculated (Appendices A–D).

For 3C 120, the average jet velocity $\langle \bar{V} \rangle \sim 2.16$ mas/year is consistent with that calculated by MOJAVE and presented on the source page in the database. The average acceleration is $\langle \bar{a} \rangle \sim -0.14$ mas/year^2, which indicates a jet slowdown and matches one of the results of [20], which finds a component slowdown starting from ∼7 mas from the core.

For 3C 273, the average jet velocity $\langle \bar{V} \rangle \sim 0.81$ mas/year was calculated (as for 3C 120), this velocity corresponds to the value proposed by MOJAVE (on the source page in the database). The average acceleration $\langle \bar{a} \rangle \sim 0.11$ mas/year^2 also was calculated.

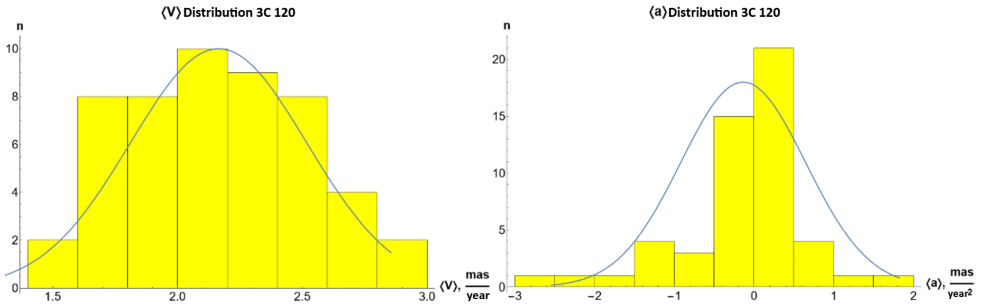


Figure 6 Histograms of distributions of average speeds (left) and accelerations (right) 3C 120 with corresponding normal distributions.

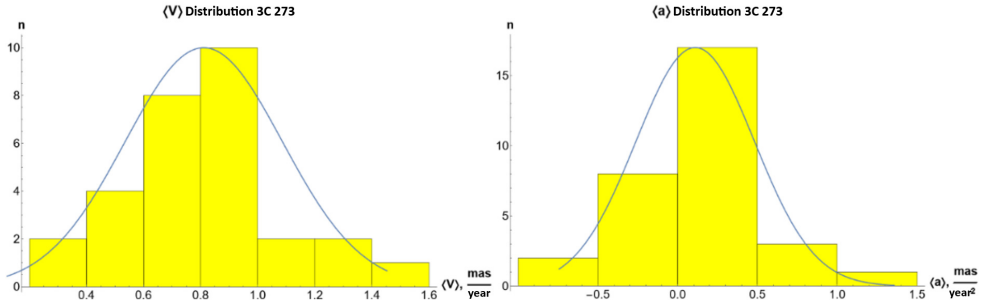


Figure 7 Histograms of distributions of average speeds (left) and accelerations (right) 3C 273 with corresponding normal distributions.

Similar to 3C 120 and 3C 273, for 3C 454.3, the average velocity $\langle \bar{V} \rangle \sim 0.19$ mas/year (corresponds to MOJAVE on the source page) and acceleration $\langle \bar{a} \rangle \sim 1.78$ mas/year^2 in the jet were estimated.

Also, for BL Lac the average jet velocity $\langle \bar{V} \rangle \sim 1.08$ mas/year and average jet acceleration $\langle \bar{a} \rangle \sim 0.28$ mas/year^2 were estimated.

For samples of average speeds (excluding quasi-stationary ones) and accelerations, standard deviations (given in Appendices A–D, as well as Table 1) were also calculated, normalized on their average values. Histograms of their distributions (together with normal distributions with these parameters) are presented in Figs 6–9.

For each component, the change in velocity over time was calculated using the filtered data (Fig. 10). The amplitude velocities were also selected as a characteristic of the component, the values of which are also given in Appendices A–D.

Also, when looking at the behavior of each component separately, we can notice certain small oscillations around the average position, whether it is a moving component or not.

This can be seen in the example of the 39th stationary component of 3C 120 (Fig. 11), where its oscillations are visible with a period of about 2.6 years and an amplitude of 0.4 to 0.8 mas relative to the mean position.

The 35th quasi-stationary component of 3C 273 oscillates around a mean position

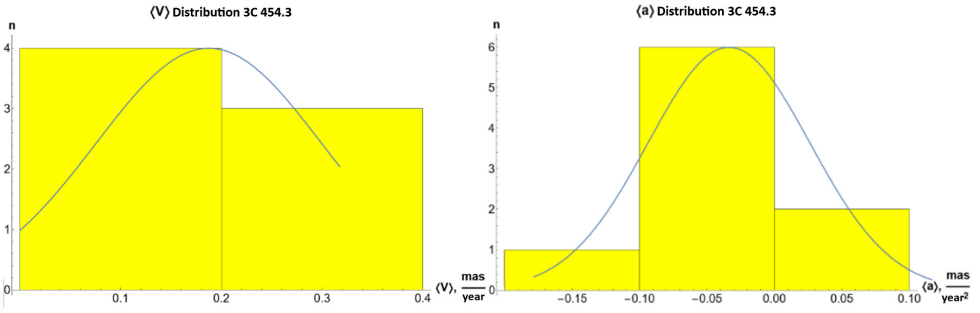


Figure 8 Histograms of distributions of average speeds (left) and accelerations (right) 3C 454.3 with corresponding normal distributions.

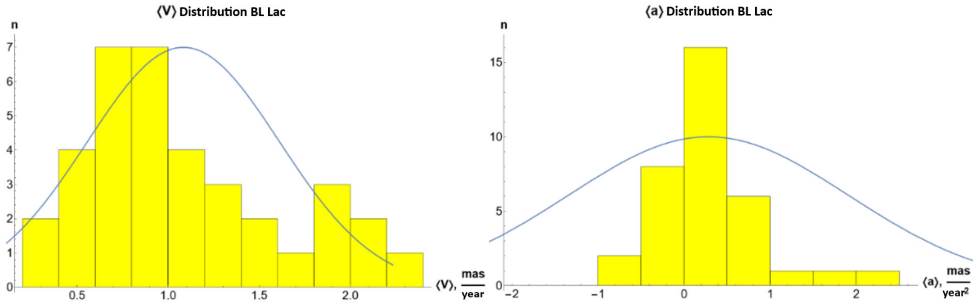


Figure 9 Histograms of distributions of average speeds (left) and accelerations (right) of BL Lac with corresponding normal distributions.

at a distance $r \sim 0.36$ mas from the core with an amplitude of ~ 0.1 mas and a period of $P \sim 1.85$ years (Fig. 12).

Since 3C 454.3 is predominantly composed of slow-moving components, it is difficult to single out any one quasi-stationary one. Most of them implement quasi-periodic motion with amplitudes <0.6 mas and periods from one to three years, as in Fig. 13.

The presence of a stationary component of BL Lac is considered in [36, 37]. The first of them describes its oscillations around the mean position with an average ~ 0.03 mas amplitude, confirmed by Fig. 14, on the left, however our Fourier spectrogram shows the main period of $P \sim 2.15$ years.

5 Discussion

The distributions of the component velocities in the jets of the Seyfert I galaxy 3C 120 and the quasar 3C 273 resemble normal ones (Figs 6 and 7), while the quasar 3C 454.3 and the BL Lac do not correspond to the normal distribution (Figs 8 and 9). In the first case, this is due to a significantly small number of components in the sample (9 components), while in the second (37 components), two peaks are identified in the

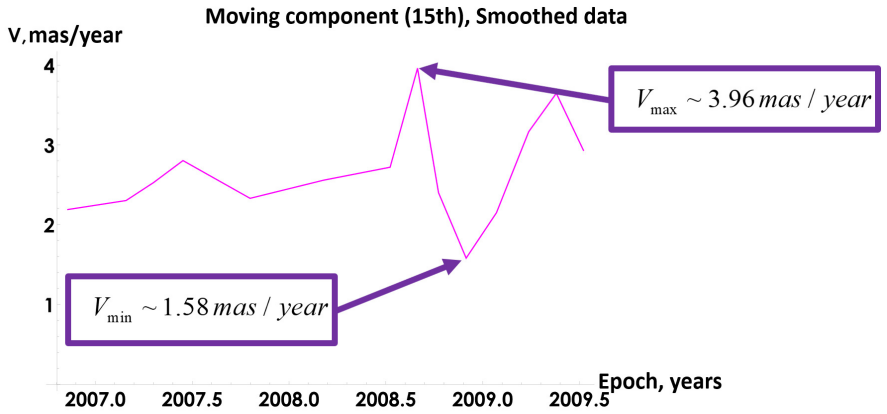


Figure 10 Change in the velocity of the 15th component over time.

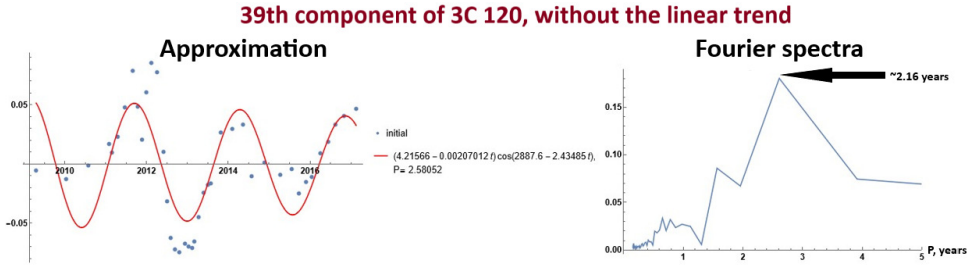


Figure 11 Quasistationary component (39th) of 3C 120 around the mean position on the left (with the linear trend excluded) with cosine approximation and Fourier transform (on the right).

histogram: from 0.5 to 1 mas/year and ∼2 mas/year, which may indicate the presence of two distinct directions (cones) in which the components are ejected into the jet (or still the effect of a small sample).

In general, the statistical parameters of the samples are presented in Table 1. Taking into account that the sources are located at different redshifts (distances), the standard deviations and average modules of the deviations of the amplitude velocities from the average for the component were normalized to the average velocities or accelerations in the jet, respectively. As a result, we will be able to compare the corresponding parameters for the jets under consideration.

The Seyfert I galaxy 3C 120 and the quasar 3C 273 show a smaller scatter in the velocities of the components in the jets than the quasar 3C 454.3 (which is sometimes classified as a blazar) and the lacertid (blazar) BL Lac. This may be due to orientation effects, so the closer the jet is to the line of sight, the less the variations in the angle at which the components are ejected will affect the observed picture.

In turn, in the two selected subgroups, 3C 273 and 3C 454.3 have a larger scatter of velocities (in comparison with 3C 120 and BL Lac, respectively). And it is about them that [23] and [30–32] (respectively) put forward reasonable assumptions about

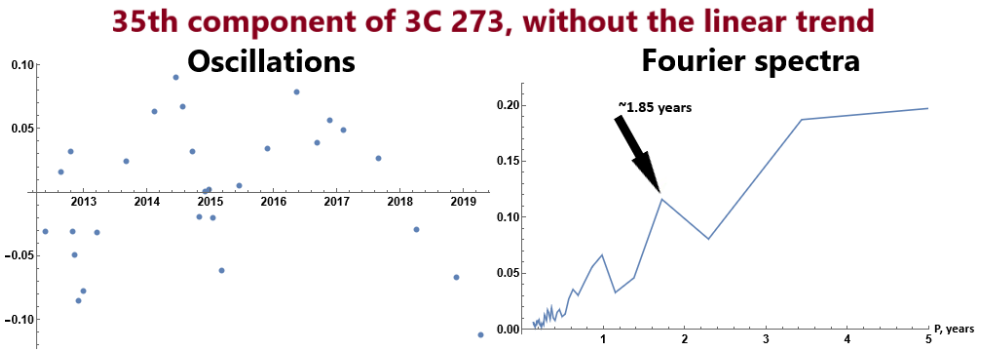


Figure 12 Oscillations of the 35th quasi-stationary component of 3C 273 around the mean position (left) and the Fourier transform (right).

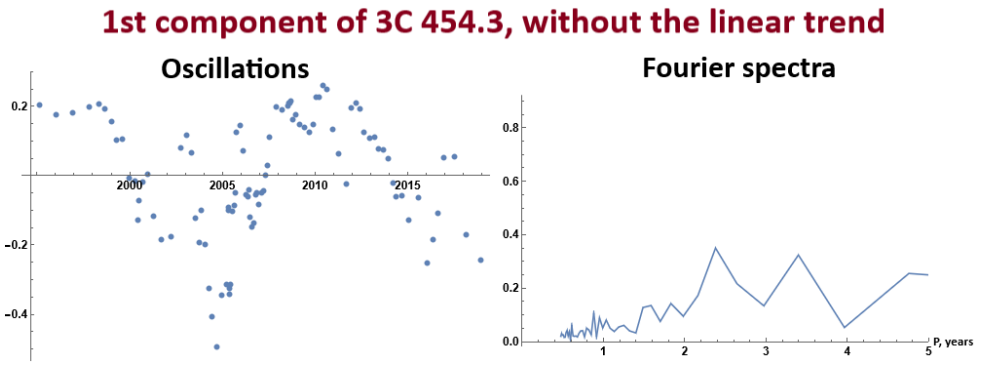


Figure 13 Oscillations of the 1st quasi-stationary component of 3C 454.3 around the mean position (left) and the Fourier transform (right).

the presence of binary black holes. This could explain the distribution of velocities by a change in the angle of component ejection to the line of sight, due to the precession of the jet caused by the presence of a companion (actually, the precession of the jets is considered in [28] and [30–32], respectively). The acceleration pattern is opposite, the reason for this is unclear.

The sign of the average acceleration in the 3C 120 jet corresponds to the result of [20], which found that the jet slows down starting from a distance of ∼7 mas (possibly this is due to the weak or absent spiral structure of the magnetic field in the jet [21], which would accelerate and collimate the components in the jet).

As one of the parameters describing the jet, the absolute deviation of the amplitude velocities $\left|V_{\max,\min} - \bar{V}\right|$ was introduced. Its average value (related to the average velocity in the jet, Table 1 or the corresponding appendices) characterizes how much the velocity of each component of the jet changes on average. Of all the components, 3C 454.3 differs the most. This may be due to the strong precession of the jet (due to the presence of one of the most massive binary black holes in AGN [30–32]) and, as a result, the general instability and shock behavior in the jet (due to constant

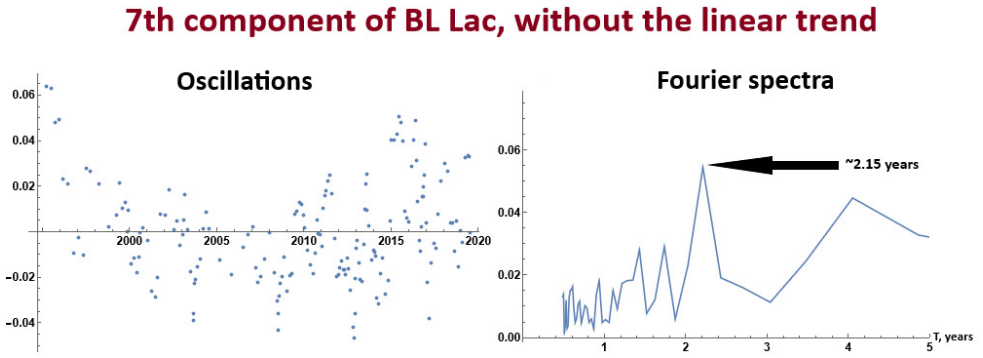


Figure 14 Oscillations of the 1st quasi-stationary component of BL Lac around the mean position (left) and the Fourier transform (right).

Table 1 Short table of statistical parameters of speed and acceleration samples.

Source	Type	$\langle \bar{V} \rangle$, $\frac{\text{mas}}{\text{year}}$	$\frac{s_{\bar{V}}}{\langle \bar{V} \rangle}$	$\langle \bar{a} \rangle$, $\frac{\text{mas}}{\text{year}^2}$	$\frac{s_{\bar{a}}}{\langle \bar{a} \rangle}$	$\left\langle \left\lvert \frac{V_{max}-\bar{V}}{\langle \bar{V} \rangle} \right\rvert \right\rangle$	$\left\langle \left\lvert \frac{V_{min}-\bar{V}}{\langle \bar{V} \rangle} \right\rvert \right\rangle$
3C 120	Seyfert 1	2.16	0.16	–0.14	5.80	0.49	0.51
3C 273	Quasar	0.81	0.34	0.11	3.39	1.11	0.96
3C 454.3	Quasar	0.19	0.60	–0.03	1.78	11.04	10.32
BL Lac	BL Lac	1.08	0.49	0.28	1.63	1.93	1.77

breaks in collimation). Either way, this is an interesting result and requires further investigation.

The observed distributions of the amplitude velocities of the components may be the result of acceleration (deceleration) of the motion of matter in the magnetic field of the jet and/or the fact that the work studies the rate of change of the distance of the components from the core in the jet without considering changes in the position angles of the components relative to the jet axis. Either way, this is something that should be paid attention to in the future.

The period of oscillations of the seventh (quasi-stationary) component of BL Lac relative to its mean position has been revised (compared to what the researchers propose in [36]). However, we consider a one-dimensional change in its distance from the core (in [36], a two-dimensional motion was considered). Therefore, its two-dimensional motion should probably be considered in further analysis.

6 Conclusions

1. The average velocities calculated are in good agreement with those provided by MOJAVE.

2. The deceleration of the 3C 120 jet ($\langle \bar{a} \rangle < 0$) was confirmed, which may be due to the absence of a strong spiral magnetic field.

3. 3C 273 and 3C 120 show distributions of average speeds close to normal.

4. The distribution of BL Lac average velocities is similar to bimodal, which may indicate the presence of two distinct ejection angles to the line of sight.

5. It was found that the average velocities of the 3C 273 and 3C 454.3 components vary more than 3C 120 and BL Lac, respectively. This may be due to the presence of double black holes in active cores and the precession of their jets.

6. It was found that of the entire sample, the components in the 3C 454.3 jet experience the largest velocity variations during their lifetime. One of the reasons may be the presence of one of the most massive binary black holes in the active core and the precession of the jet.

7. A different period of oscillation of the stationary component (7th) in lacertids BL Lac (2.15 years) is proposed.

References

[1] Brandon C. Kelly, Philip A. Hughes, Hugh D. Aller, Margo F. Aller. The Cross-Wavelet Transform and Analysis of Quasi-periodic Behavior in the Pearson-Readhead VLBI survey sources. The Astrophysical Journal, 2003, Vol. 591, Issue 2, P. 695-713.

[2] Begelman M. C., Blandford, R. D., Rees, M. J. Massive black hole binaries in active galactic nuclei. Nature, 1980, Vol. 287, Issue 5780, P. 307-309.

[3] A.P. Marcher. Jets in Active Galactic Nuclei. 2009. https://arxiv.org/abs/0909.2576

[4] Ryan Tanner, Kimberly Weaver. Simulations of AGN-driven Galactic Outflow Morphology and Content. 2022. https://arXiv: 2201.08360

[5] https://science.nrao.edu/facilities/vlba/docs/manuals/oss/ang-res.

[6] https://www.cv.nrao.edu/MOJAVE/allsources.html.

[7] M.L. Lister, M.H. Cohen, D.C. Homan et al. MOJAVE: Monitoring of Jets in Active Galactic Nuclei with VLBA Experiments. VI. Kinematics Analysis of a Complete Sample of Blazar Jets. 2009. https://arxiv.org/abs/0909.5100.

[8] M.L. Lister, D.C. Homan, T. Hovatta et al. MOJAVE. XVII. Jet Kinematics and Parent Population Properties of Relativistically Beamed Radio-loud Blazars. 2009. https://arxiv.org/abs/1902.09591.

[9] M.L. Lister, D.C. Homan, K.I. Kellermann et al. Monitoring of Jets in Active Galactic Nuclei with VLBA Experiments. XVIII. Kinematics and Inner Jet Evolution of Bright Radio-loud Active Galaxies. The Astrophysical Journal, 2021, Vol. 923, Issue 1, id 30.

[10] A.L. Sukharev, M.I. Ryabov, V.V. Bezrukovs. Property Study of OJ 287 and BL Lac Variability in Optical and Radio Ranges. Radio physics and radio astronomy, 2019, Vol. 24, No. 4, P.254-271.

[11] A.L. Sukharev. Variability of the Extragalactic Radio Sources 3C 446 and BL Lac in the Centimeter Wavelength Range. Astrophysics, 2015, Vol. 58, No. 1, P.5-18.

[12] Suharev A.L., Ryabov M.I., Donskix A.I., Aller M. Variability flux of extragalactic sources DA55, CTA 102, 3C 120 AND OJ 287 in microwave range. Astronomical School's Report, 2013, Vol. 9, No. 1, P. 85-92.

[13] Ryabov M.I., Sukharev A.L. The use of different methods of determining the periods of variability of extragalactic radio sources 3C120, 3C345, OJ287 at 30 years of observations at centimeter wavelengths. Astronomical School's Report, 2009, Vol. 6, No. 2, - P.174-180.

[14] Sukharev A.L., Ryabov M.I., Donskikh G.I. Predicting Changes in the Radio Emission Fluxes of Extragalactic Sources. Astrophysics, 2016, Vol. 59, P.213–226.

[15] Zabora D., Ryabov M., Sukharev A. et al. On the perspectives for separating the radio flux variations of the nucleus and the jet of active galactic based on data from monitoring programs and VLBI observations. Astronomical and Astrophysical Transactions, 2022, Vol. 33, Issue 1, P.89–100.

[16] Zabora D., Ryabov M., Sukharev, A. et al. Motions of the Components of AGNS According to VLBI Mojave Data as Indicators of the Activity and Spatial Structure of the Jet. Odessa Astronomical Publications, 2023, Vol. 36, P.154-160.

[17] Burbidge E.M. Redshifts of Thirteen Radio Galaxies. The Astrophysical Journal, 1967, Vol. 149., №2, P.51-54.

[18] Michael Hlabathe, David Starkey, Keith Horne et al. Robotic reverberation mapping of the broad-line radio galaxy 3C 120. MNRAS, 2020, Vol. 497, Issue 3, P.2910-2929.

[19] Zdziarski A.A., Phuravhathu D.G., Sikora M et al. The Composition and Power of the Jet of the Broad-line Radio Galaxy 3C 120. The Astrophysical Journal Letters, 2022, Vol. 928, L9, p.6.

[20] F. Mertens, A.P. Lobanov. Detection of multiple velocity components in partially overlapping emitting regions. 2016. https://arxiv.org/abs/1601.05926.

[21] Gómez J.L., Casadio C., Roca-Sogorb Mar et al. Helical Magnetic Fields in Relativistic Jets Through Faraday Rotation and Jet Stratification Studies. International Journal of Modern Physics: Conference Series, 2012, Vol. 8., P. 265-270.

[22] Schmidt M. 3C 273: A Star-Like Object with Large Red-Shift. Nature, 1963, Vol 197, P.1040.

[23] Volvach A., Volvach L., Larionov M. A Close Binary Supermassive Black Hole Model for the Galaxy 3C 273. Galaxies, 2023, Vol. 11, Issue 5, p.13.

[24] Paltani S., Turler M. The mass of the black hole in 3C 273. Astronomy & Astrophysics, 2005, Vol. 435, №3, P.811-820.

[25] Hiroki Okino, Kazunori Akiyama, Keiichi Asada et al. Collimation of the Relativistic Jet in the Quasar 3C273. The Astrophysical Journal, 2022, Vol. 940, Issue 1, pp.17.

[26] Akiyama, K. Asada, K., Fish, V.L. et al. The Global Jet Structure of the Archetypical Quasar 3C 273. Galaxies 2018, Vol. 6, Issue 1, pp. 7.

[27] T. Savolainen, K. Wiik, E. Valtaoja et al. Multifrequency VLBA monitoring of 3C 273 during the INTEGRAL Campaign in 2003. I. Kinematics of the parsec scale jet from 43 GHz data. Astronomy & Astrophysics, 2006, Vol. 446, Issue 1, P.71-85.

[28] Qian, S.-J., Zhang, X.-Z., Krichbaum T. P. Periodic Variations of the Jet Flow Lorentz Factor in 3C 273. Chinese Journal of Astronomy & Astrophysics, 2001, Vol. 1, №3, P.236-244.

[29] Jackson N., Browne I.W.A. Optical properties of quasars – I. Observations. MNRAS, 1991, Vol. 250, Issue 2, P.414-421.

[30] Volvach A.E., Volvach L.N., Larionov M.G. Most massive double black hole 3C 454.3 and powerful gravitational wave radiation. Astronomy & Astrophysics, 2021, Vol. 643, id A27. – p.8.

[31] Qian S. J., Britzen S., Krichbaum, T. P et al. Possible evidence for a supermassive binary black hole in 3C454.3. Astronomy & Astrophysics, 2021, Vol. 653, id A7, p.22.

[32] S.J.Qian. Flux evolution of superluminal components in blazar 3C454.3. https://arxiv.org/abs/2306.06863.

[33] Motter J.C., Gabuzda D.C. 18-22 cm VLBA Faraday rotation studies of six AGN jets. MNRAS, 2017, Vol. 467, Issue 3. P.2648-2663.

[34] Vermeulen R.C., Ogle P.M., Tran H.D et al. When Is BL Lac Not a BL Lac. The Astrophysical Journal, 1995, Vol. 425, P. L5-L8.

[35] Titarchuk L., Seifina E. BL Lacertae: X-ray spectral evolution and a black-hole mass estimate. Astronomy & Astrophysics, 2017, Vol. 602, id A113, p.16.

[36] Hambardzumyan L.A., Arshakian T.G., Pushkarev A.B. BL Lacertae: a study of quasi-stationary feature trajectories in the inner part of a relativistic jet. Communications of the Byurakan Astrophysical Observatory, 2023, Vol. 70, Issue 1, P.94-99.

[37] Cohen M.H., Meier D.L., Arshakian T.G. et al. Studies of the Jet in Bl Lacertae. I. Recollimation Shock and Moving Emission Features. The Astrophysical Journal, 2014, Vol. 787, Issue 2, id A151, p.10.

[38] J.L. Gómez, A.P. Lobanov, G. Bruni et al. Probing the Innermost Regions of AGN Jets and Their Magnetic Fields with RadioAstron. I. Imaging BL Lacertae at 21 Microarcsecond Resolution. The Astrophysical Journal, 2016, Vol. 817, Issue 2, id. A96, p.14.

Appendix A. Table of kinematic parameters of 3C 120 components.

No	Time interval, years	Duration, years	$\bar{V}$, $\frac{\text{mas}}{\text{year}}$	$\bar{a}$, $\frac{\text{mas}}{\text{year}^2}$	$V_{\max}$, $\frac{\text{mas}}{\text{year}}$	$V_{\min}$, $\frac{\text{mas}}{\text{year}}$
1	2001.–2002.19	1.19	2.14	1.72	2.95	0.19
2	1996.93–2002.19	5.25	1.70	–0.07	2.43	0.50
3	2001.–2002.19	1.19	2.31	0.83	2.71	1.58
4	2001.09–2002.19	1.1	1.92	1.30	2.47	–0.16
5	2000.49–2002.19	1.7	1.81	0.53	2.41	0.05
6	2000.49–2002.19	1.7	1.84	0.25	4.32	–0.64
7	2001.–2002.19	1.19	2.10	0.11	3.06	1.38
8	2001.09–2002.19	1.1	1.49	–0.16	2.02	0.42
11	2003.66–2010.53	6.87	2.31	0.17	4.51	1.30
12	2003.1–2007.62	4.52	2.29	0.38	4.95	1.34
13	2004.8–2013.24	8.44	2.35	–0.19	5.81	0.55
14	2005.73–2009.23	3.5	2.62	0.38	6.97	2.07
15	2006.39–2009.51	3.12	2.60	0.20	3.96	1.58
17	2007.16–2014.43	7.26	2.43	–0.13	4.74	–0.59
21	2001.44–2002.19	0.75	0.05	–0.49	0.42	–0.31
22	1995.57–2001.	5.43	1.79	0.05	2.31	1.25
24	1995.57–1998.84	3.26	1.97	–0.12	2.79	1.20
25	1996.23–1998.18	1.95	1.83	0.06	2.18	1.19
28	2003.1–2005.02	1.92	2.25	–	2.85	1.92
29	2003.1–2007.16	4.07	1.93	0.05	2.01	1.78
30	2003.1–2006.39	3.3	2.39	0.02	2.51	2.18
31	2006.39–2009.23	2.84	2.85	–0.22	3.38	2.18
32	2008.33–2012.84	4.51	2.59	–0.28	4.19	–1.30
33	2008.33–2009.23	0.89	1.68	0.80	2.15	0.58
35	2008.91–2009.63	0.72	1.76	–0.66	1.95	1.16
36	2009.08–2012.33	3.25	2.42	0.41	3.41	1.54
37	2009.08–2010.11	1.03	1.82	–1.30	2.37	1.28
38	2009.4–2012.33	2.92	2.54	0.15	3.62	1.81
39	2009.51–2017.19	7.68	–0.02	0.01	0.40	–0.50
41	2009.94–2014.03	4.09	2.65	0.37	3.51	1.51
42	2010.91–2011.75	0.84	1.76	–2.54	3.89	0.37
43	2010.53–2011.18	0.65	2.41	–1.72	3.14	1.88
44	2010.53–2012.18	1.65	2.11	–0.24	2.97	1.32
45	2011.38–2014.88	3.5	2.18	–0.27	3.40	0.82
47	2012.33–2019.49	7.16	2.33	0.10	3.59	1.23
50	2012.33–2014.88	2.55	2.85	0.23	4.09	2.10
51	2016.18–2017.19	1.01	1.74	–1.49	2.61	0.90
54	2014.24–2019.49	5.25	2.18	0.31	3.64	–0.46
55	2013.52–2015.75	2.23	1.55	0.16	2.67	0.82
56	2014.03–2015.75	1.72	1.66	–0.22	3.02	0.96
57	2015.38–2016.18	0.8	2.48	–1.33	3.22	1.79
58	2015.55–2016.42	0.88	2.05	0.14	2.25	1.69

continued on next page

Appendix A continued

No	Time interval, years	Duration, years	$\bar{V}$, $\frac{\text{mas}}{\text{year}}$	$\bar{a}$, $\frac{\text{mas}}{\text{year}^2}$	$V_{\max}$, $\frac{\text{mas}}{\text{year}}$	$V_{\min}$, $\frac{\text{mas}}{\text{year}}$
59	2016.39–2017.65	1.26	2.37	–0.55	3.11	1.08
60	2016.39–2017.65	1.26	2.14	–0.29	3.09	1.36
61	2016.83–2019.29	2.46	2.08	–0.50	3.29	0.64
62	2012.39–2014.43	2.03	2.41	–1.39	5.70	–0.30
67	2015.38–2019.45	4.07	2.16	0.06	3.00	1.33
68	2016.99–2017.4	0.41	1.74	–	2.08	0.68
69	2017.46–2018.63	1.17	2.03	0.33	2.71	1.87
70	2017.4–2018.63	1.24	1.99	0.81	2.81	1.53
71	2018.31–2019.05	0.74	2.80	–2.36	3.20	1.19
72	2018.31–2019.55	1.24	2.32	–0.11	3.07	–0.47
75	2018.52–2019.29	0.77	0.04	–0.23	0.12	–0.04
77	2016.39–2019.45	3.06	2.70	–0.06	4.09	1.31

Notes:

average jet speed $\left\langle \bar{V} \right\rangle \sim 2.16 \frac{\text{mas}}{\text{year}}$, $\frac{s_{\bar{V}}}{\left\langle \bar{V} \right\rangle} \sim 0.16$

average jet acceleration $\langle \bar{a} \rangle \sim -0.14 \frac{\text{mas}}{\text{year}^2}$, $\frac{S_{\bar{a}}}{|\langle \bar{a} \rangle|} \sim 5.8$

average $\left\langle \left| \frac{V_{\max} - \bar{V}}{\left\langle \bar{V} \right\rangle} \right| \right\rangle \sim 0.49$

average $\left\langle \left| \frac{V_{\min} - \left\langle \bar{V} \right\rangle}{\left\langle \bar{V} \right\rangle} \right| \right\rangle \sim 0.51$

Appendix B. Table of kinematic parameters of 3C 273 components.

No	Time interval, years	Duration, years	$\bar{V}$, $\frac{\text{mas}}{\text{year}}$	$\bar{a}$, $\frac{\text{mas}}{\text{year}^2}$	$V_{\max}$, $\frac{\text{mas}}{\text{year}}$	$V_{\min}$, $\frac{\text{mas}}{\text{year}}$
1	1995.57– 2000.33	4.76	0.79	0.16	2.78	–0.29
2	1995.57–2009.55	13.99	0.79	0.04	4.10	–1.14
3	1995.57–2000.61	5.04	1.04	–0.11	2.01	0.40
4	1995.57–1996.93	1.36	1.32	0.31	1.75	0.84
5	1995.57–2000.61	5.04	1.45	0.02	2.07	0.73
6	1995.85–1996.93	1.09	0.99	0.11	1.15	0.83
7	1996.37–1996.93	0.56	0.64	0.60	0.79	0.42
8	1997.66–1999.74	2.08	0.49	0.04	1.51	–0.23
9	1998.83–2019.28	20.45	1.07	0.01	2.20	–0.32
12	2001.99–2019.28	17.29	0.93	0.01	2.41	–0.48
13	2002.74–2004.92	2.18	0.59	0.00	0.78	0.17
15	2004.44–2007.29	2.85	0.90	0.33	2.14	0.13
16	2005.38–2007.29	1.91	0.63	–0.74	1.08	0.04
17	2006.45–2007.29	0.84	0.31	1.26	0.68	–0.22
18	2005.87–2007.29	1.42	0.24	0.36	0.57	0.06
19	2008.33–2010.89	2.55	0.74	–0.11	1.40	–0.01
21	2001.99–2006.92	4.93	0.50	0.01	1.02	–0.16
22	2009.65–2019.28	9.63	0.92	0.03	1.72	0.41
24	2008.33–2009.92	1.59	0.71	0.27	1.26	0.32
25	2008.33–2009.92	1.59	0.51	0.72	1.16	–0.22
26	2001.2–2019.28	18.09	0.99	0.00	3.28	–0.53
27	1997.66–2000.61	2.95	1.21	–0.50	2.02	0.03
29	2008.33–2019.28	10.95	0.73	–0.03	3.60	–0.92
30	2010.07–2014.42	4.36	0.88	–0.10	2.07	0.53
31	2010.82–2015.35	4.53	0.81	0.01	1.66	0.10
32	2012.32–2013.95	1.63	0.14	–0.08	0.31	–0.25
35	2012.32–2019.28	6.96	0.00	–0.02	0.24	–1.96
36	2016.74–2019.28	2.55	0.97	–0.03	1.48	0.66
37	2013.95–2019.28	5.33	0.93	–0.12	1.64	0.44
38	2015.9–2019.28	3.39	0.83	0.10	1.68	–0.24
39	2015.9–2017.39	1.5	0.60	0.86	1.09	0.28

Notes:

average jet speed $\langle \bar{V} \rangle \sim 0.81 \frac{\text{mas}}{\text{year}}$, $\frac{s_{\bar{V}}}{\langle \bar{V} \rangle} \sim 0.34$

average jet acceleration $\langle \bar{a} \rangle 0.11 \frac{\text{mas}}{\text{year}^2}$, $\frac{S_{\bar{a}}}{|\langle \bar{a} \rangle|} \sim 3.4$

average $\left\langle \left| \frac{V_{\max} - \bar{V}}{\langle \bar{V} \rangle} \right| \right\rangle \sim 1.11$

average $\left\langle \left| \frac{V_{\min} - \langle \bar{V} \rangle}{\langle \bar{V} \rangle} \right| \right\rangle \sim 0.96$

Appendix C. Table of kinematic parameters of 3C 454.3 components.

No	Time interval, years	Duration, years	$\bar{V}$, $\frac{\text{mas}}{\text{year}}$	$\bar{a}$, $\frac{\text{mas}}{\text{year}^2}$	$V_{\max}$, $\frac{\text{mas}}{\text{year}}$	$V_{\min}$, $\frac{\text{mas}}{\text{year}}$
1	1995.4–2018.86	23.46	0.0450	0.00	2.33	–10.41
2	1995.4–2018.86	23.46	0.0502	0.00	3.30	–1.39
3	2005.32–2010.05	4.72	0.1826	–0.01	2.94	–0.14
4	2005.32–2014.58	9.25	0.2506	–0.03	6.09	–0.60
5	2001.06–2010.88	9.83	0.1592	–0.01	1.60	–3.16
8	2005.32–2007.31	1.99	0.3172	–0.18	2.51	–0.10
13	2008.48–2010.74	2.25	0.0120	0.02	0.58	-0.35
18	2011.27–2014.58	3.31	0.0150	–0.08	0.27	–0.18
23	2016.44–2018.86	2.42	0.3074	–0.02	0.35	0.28

Notes:

average jet speed $\left\langle \bar{V} \right\rangle \sim 0.19 \frac{\text{mas}}{\text{year}}$, $\frac{s_{\bar{V}}}{\left\langle \bar{V} \right\rangle} \sim 0.6$

average jet acceleration $\langle \bar{a} \rangle \sim -0.03 \frac{\text{mas}}{\text{year}^2}$, $\frac{S_{\bar{a}}}{|\langle \bar{a} \rangle|} \sim 1.78$

average $\left\langle \left| \frac{V_{\max} - \bar{V}}{\left\langle \bar{V} \right\rangle} \right| \right\rangle \sim 11.04$

average $\left\langle \left| \frac{V_{\min} - \left\langle \bar{V} \right\rangle}{\left\langle \bar{V} \right\rangle} \right| \right\rangle \sim 10.32$

Appendix D. Table of kinematic parameters of BL Lac components.

No	Time interval, years	Duration, years	$\bar{V}$, $\frac{\text{mas}}{\text{year}}$	$\bar{a}$, $\frac{\text{mas}}{\text{year}^2}$	$V_{\max}$, $\frac{\text{mas}}{\text{year}}$	$V_{\min}$, $\frac{\text{mas}}{\text{year}}$
1	1999.–2000.99	1.99	2.01	0.06	4.27	0.16
1	1995.4–2018.86	23.46	0.0450	0.00	2.33	–10.41
2	1999.–1999.85	0.84	1.04	1.83	1.66	0.64
3	1999.37–2001.84	2.46	0.89	0.52	2.63	-1.17
4	1999.–2004.69	5.69	1.16	0.25	8.40	-4.39
5	1999.37–2004.08	4.71	0.76	0.47	3.40	–0.49
6	2000.31–2004.08	3.77	0.71	0.56	2.47	–1.37
7	1995.26–2019.54	24.28	0.00	0.00	0.53	–0.68
8	1999.79–2003.24	3.46	1.42	-0.50	4.45	–5.61
10	2001.97–2004.08	2.11	0.99	0.63	4.25	–1.76
11	2003.63–2007.24	3.6	1.90	0.12	3.17	–0.60
12	2003.74–2007.24	3.5	1.23	0.11	5.82	–0.71
13	2004.0–2007.24	3.16	1.09	0.09	1.63	0.32
14	2006.26–2007.44	1.18	0.97	–0.87	1.38	–0.49
15	2005.71–2007.24	1.53	0.83	0.01	1.30	0.69
16	2005.71–2008.58	2.87	0.94	0.45	1.68	–0.50
19	2008.33–2010.05	1.71	1.88	0.99	4.77	0.80
20	2008.33–2014.95	6.62	0.79	–0.10	2.98	–9.23
23	2008.48–2014.24	5.76	0.61	–0.03	5.50	–0.74
24	2008.89–2011.69	2.81	0.52	0.11	2.00	–0.12
25	2009.15–2011.69	2.55	0.49	0.22	2.08	–0.66
26	2011.27–2012.98	1.7	0.88	0.42	1.72	–1.00
27	2011.99–2013.61	1.62	1.03	–0.40	6.63	–1.27
28	2008.03–2008.58	0.55	1.58	1.07	2.12	0.24
34	2008.65–2009.72	1.08	2.07	0.61	2.69	1.33
36	2012.98–2013.63	0.66	1.81	–0.12	6.44	0.20
38	2011.99–2012.67	0.68	0.46	2.36	1.44	–0.68
39	2012.48–2013.11	0.63	0.87	0.56	2.52	–1.53
45	2015.96–2018.95	2.99	0.56	-0.03	1.63	–2.76
46	2015.96–2019.45	3.48	1.78	–0.08	5.65	–0.43
47	2013.95–2017.65	3.69	1.36	0.15	7.54	–1.09
49	2013.95–2014.24	0.29	0.26	6.80	0.80	–0.81
52	2013.24–2013.63	0.39	2.23	–6.10	3.35	0.92
60	2016.94–2019.45	2.5	0.80	0.01	2.87	0.13
61	2017.3–2018.3	1	0.31	–0.20	0.66	0.05
62	2017.46–2018.3	0.84	0.79	0.26	0.88	0.51
67	2017.07–2019.54	2.47	0.63	0.32	3.21	–0.60
68	2018.41–2018.95	0.54	1.32	–0.07	1.79	0.76

Notes:

average jet speed $\left\langle \bar{V} \right\rangle \sim 1.08 \frac{\text{mas}}{\text{year}}$, $\frac{s_{\bar{V}}}{\left\langle \bar{V} \right\rangle} \sim 0.49$

average jet acceleration $\langle \bar{a} \rangle \sim 0.28 \frac{\text{mas}}{\text{year}^2}$, $\frac{S_{\bar{a}}}{|\langle \bar{a} \rangle|} \sim 1.63$

average $\left\langle \left| \frac{V_{\max} - \bar{V}}{\left\langle \bar{V} \right\rangle} \right| \right\rangle \sim 1.93$

average $\left\langle \left| \frac{V_{\min} - \left\langle \bar{V} \right\rangle}{\left\langle \bar{V} \right\rangle} \right| \right\rangle \sim 1.77$